Magnetization relaxation and search for the magnetic gap in bulk-insulating V-doped $(Bi, Sb)_2Te_3$

E. Golias[1,+], E. Weschke[1], T. Flanagan[2], E. Schierle[1], A. Richardella[2], E. D. L. Rienks[1,3,4],

P. S. Mandal[1], A. Varykhalov[1], J. Sánchez-Barriga[1], F. Radu[1], N. Samarth[2], O. Rader[1,*]

[1]*Helmholtz-Zentrum Berlin für Materialien und Energie,*

Elektronenspeicherring BESSY II, Albert-Einstein-Straße 15, 12489 Berlin, Germany

[2]*Department of Physics, Pennsylvania State University, University Park, PA 16802, USA*

[3]*Institut für Festkörperphysik, Technische Universität Dresden, 01062 Dresden, Germany*

[4]*Leibniz-Institut für Festkörper- und Werkstoffforschung Dresden,*

Helmholtzstraße 20, 01069 Dresden, Germany

[+]*Present address: MAX IV Laboratory, Lund University,*

Fotongatan 2, 22484 Lund, Sweden and

[*]*Corresponding author. Email: rader@helmholtz-berlin.de*

(Dated: September 10, 2021)

Abstract

V-doped $(Bi,Sb)_2Te_3$ has a ten times higher magnetic coercivity than its Cr-doped counterpart and therefore is believed to be advantageous for the quantum anomalous Hall effect (QAHE). The QAHE requires the opening of a magnetic band gap at the Dirac point. We do not find this gap by angle-resolved photoelectron spectroscopy down to 1 K. By x-ray magnetic circular dichroism (XMCD) we directly probe the magnetism at the V site and derive spin and orbital magnetic moments of 1.69 and -0.22 μ_B/atom. Hysteresis curves of the XMCD signal show a strong dependence of the coercivity on the ramping velocity of the magnetic field. The XMCD signal decays on a time scale of minutes which we conclude contributes to the absence of a detectable magnetic gap at the Dirac point.

1

Magnetically doped topological insulators are expected to give rise to a range of new phenomena due to the opening of a magnetic gap at the Dirac point of the topologically protected surface state. The quantum anomalous Hall effect (QAHE), demonstrated in 2013 [1], is characterized by a quantized Hall resistance $\rho_{xy} = h/(Ne^2)$ with N an integer number of edge channels. These permit lossless charge transport in Cr- and V-doped $(Bi,Sb)_2Te_3$ [1–9]. V-doped $(Bi,Sb)_2Te_3$ was early on found to reach high Curie temperatures of 17 K [10] and even much higher temperatures were reported for metallic V concentrations such as 17% V in Sb_2Te_3 (up to 177 K [11]). One advantage of V is that despite its relatively small magnetic moment, its T_C is high due to the high density of states at the Fermi level meaning a high exchange integral [12]. A high V density of states was found near the Fermi energy (0.1 to 0.2 eV binding energy [13]), using resonant photoemission at the V L_3 edge [13, 14]. By resonant angle-resolved photoemission (ARPES), the V contribution was identified as nondispersing impurity band and found consistent with calculations for V occupying Bi-substitutional sites [13].

Another advantage is the coercivity H_c. It is ~ 0.1 T for Cr-doped $(Bi,Sb)_2Te_3$ [1, 4, 5] while for the V-doped system $H_c \sim 1.3$ T ($T = 2$ K) [8]. The high coercivity is believed to lead to a very homogeneous ferromagnetism with much smaller number of domains that leads to perfect edge state formation [8]. This property facilitated the achievement of perfect quantization of ρ_{xy} with a precision of $\pm 6 \times 10^{-4}$ h/e^2 and ρ_{xx} as low as 3.35 ± 1.76 Ω [8]. We note that in current state-of-the-art devices, both Cr- and V-doped $(Bi,Sb)_2Te_3$ samples now show precisely quantized Hall resistance to sub-ppm precision [15, 16].

A decisive parameter that determines the temperature scale for observing the QAHE is the magnetic band gap at the Dirac point which is caused by the exchange interaction. A magnetic gap that protects the edge states of the QAHE can be deduced from the thermal activation of dissipation-free transport. However, in V- and Cr-doped QAHE samples, this gap is in the range 50-100 μeV, orders of magnitude lower than the principal limit set by T_C [17], even when considering the highest temperatures around 1 K achieved with the help of a depth-dependent concentration profile of Cr impurities [18].

For V-doped Sb_2Te_3, Landau level spectroscopy has been performed by scanning tunneling spectroscopy at 1.3 K [19]. The method requires the application of high magnetic fields, hence a comparison of samples with and without V doping was used to derive a mobility gap which amounts to 32 meV. This gap does, however, not appear in the local density of states,

possibly due to overlap with impurity states [19]. For Cr-doped $(Bi,Sb)_2Te_3$, an average gap of 56 meV was found by tunneling spectroscopy [20]. Its origin could not be related to magnetism because only data at a single temperature of 4.5 K are available. In ARPES, a large gap at the Dirac point of $\sim$75 meV was found for Cr-doped Bi_2Se_3 even at room temperature, i. e., far above T_C [21]. These gaps are therefore not of magnetic origin. In a $V_{0.04}Bi_{1.96}Se_3$ epitaxial film, ARPES at 100 K showed the opening of a gap in the surface state of 180 meV at the Dirac point at ~ 0.3 eV binding energy [22]. It was concluded that this gap is not of magnetic origin because a ferromagnetic Curie temperature of 10 K was measured [22]. The composition of insulating $(Bi,Sb)_2(Te,Se)_3$ can vary strongly between epitaxial films and single crystals. This holds also for V-doped systems where the composition $V_{0.015}Bi_{1.985}Se_{0.6}Te_{2.4}$ has the Dirac point at 0.33 eV and $V_{0.03}Bi_{1.97}Se_{0.6}Te_{2.4}$ at 0.38 eV binding energy [23]. ARPES of an insulating V-doped $(Bi,Sb)_2Te_3$ epitaxial film showed that the Dirac point is degenerate with the bulk valence band and it was concluded that this limits the achievable temperature of the QAHE [24]. No magnetic gap could be found in this system, $(Bi_{0.29}Sb_{0.71})_{1.89}V_{0.11}Te_3$, down to 7 K [24]. Recently, Cr-doped $(Bi,Sb)_2Te_3$ was studied by ARPES at 12 K after surface n-doping by potassium and no magnetic gap was found [25].

In the present work we undertake a search for the magnetic gap of V-doped $(Bi, Sb)_2Te_3$ at the Dirac point down to 1 K. Moreover, we investigate the magnetization behavior of the same sample directly and element specifically through magnetic x-ray dichroism (XMCD) in soft x-ray absorption and reflectivity.

Samples were grown by molecular beam epitaxy (MBE) from single elemental sources of at least 5N purity. The InP(111) substrate was mounted by indium on the MBE sample holder. A V-doped $(Bi, Sb)_2Te_3$ sample of 10 quintuple layer (QL) thickness was grown at 240°C with a growth rate of about 0.5 QL per minute. The sample was capped with 2 nm Te for protection against ambient influence and to allow in situ removal of the cap for ARPES. The sample was cut into pieces with a diamond cutter to be able to studuy the same sample by the various experimental methods. For transport, magnetization, and soft-x-ray experiments, the cap was kept in place. For the ARPES experiment, the cap was removed in situ by noble gas ion sputtering and annealing. Photoemission experiments were performed with the ARPES-1[3] end station at the UE112-PGM2b undulator beam line of the BESSY II synchrotron radiation source. In this instrument, the sample can be cooled to 1 K.

The experimental geometry is the following: With the central axis of the analyser lens and the polar rotation axis of the sample defined as the x and z axes of a spherical coordinate system, the photon beam is incident on the sample under an azimuthal angle of 45° and a polar angle of 84°. The light polarization is horizontal (along the x axis). The entrance slit of the hemispherical analyser is placed parallel to the z axis. The measurements at $h\nu = 105$ eV were performed with an energy resolution of 10 meV. XMCD was performed at the High-Field and XUV diffractometers of the UE46-PGM1 undulator beam line of BESSY II. Spectra were taken around the V-$L_{2,3}$ excitation energy for incident photons with opposite circular polarization and recording the total electron yield through the sample current. The High-Field setup provides fields up to 7 T by means of a superconducting Helmholtz-coil-like arrangement. The magnetic field is applied in the direction of the light incidence, this is along the surface normal in Fig. 3(a) and under 45° in Fig. 3(b–f).

Transport measurements were carried out on a mechanically defined (scratched) Hall bar of dimensions 1 mm × 0.5 mm. At 4.5 K, the longitudinal magnetoresistance $\rho_{xx}(H)$ shows peaks at the coercive field, Fig. 1(a), while the transverse magnetoresistance $\rho_{xy}(H)$ shows a square hysteresis loop, Fig. 1(b). This behavior is typical for a QAHE sample above the temperature required for perfect quantization. From the hysteresis measurements, enlarged in Fig. 1(c), we derive a Curie temperature of 25 K in agreement with additional superconducting quantum interference device (SQUID) measurements (data not shown). Note that finite remanent Hall resistance at zero magnetic field is only observed after first saturating the magnetization of the sample at a field greater than the coercivity: when cooled down in zero field, such samples do not show any significant spontaneous zero field Hall resistance due to the formation of randomly oriented magnetic domains.

ARPES data at 1, 20, and 40 K cover the range well below and well above T_{C} as determined from Fig. 1. The angle (respectively $\mathbf{k}_\parallel$) dependence as well as the normal emission ($\mathbf{k}_\parallel = 0$ Å^{-1}) spectrum display an intensity maximum at ~ 0.15 eV binding energy. This is due to matrix element effects and can approximately be explained as final-state effect when sampling the bulk band structure with varying photon energy. The magnetic band gap at the Fermi level requires magnetization perpendicular to the surface plane [26] and scales with the magnetization [27]. Due to the insulating character, the Dirac point is expected to be at the Fermi level. Nevertheless, no gap appears in the data of Fig. 2 with an upper limit of ~ 5 meV. In order to independently estimate the position of the Dirac point, we analyzed

the width of the momentum distribution curves (MDC). Figure 2(b) shows the same data as Fig. 2(a) but as MDC. We fit the MDC near the narrowest point with a single Lorentzian component the full width at half maximum of which is plotted in Fig. 2(d). We arrived at $E_D \approx 50$ meV. This indicates a small extent of band bending and is interestingly in good agreement with the result by Li et al. for insulating samples who located the Dirac point at 54 meV binding energy [24].

XMCD is the method of choice to derive element specific magnetization. It does not require to take into account transport effects as in magnetotransport or sample and substrate diamagnetism as in SQUID magnetometry. The XMCD spectrum in Fig. 3(a) displays the L_2 and L_3 edges which are not fully separated for V. The spectrum resembles the one obtained from bulk crystals of V-doped Sb_2Te_3 [19, 28]. We performed a sum-rule analysis [29] including the corrections for the overlap of L_2 and L_3 edges and the dipole term by Tcakaev et al. [30]. We derive a spin magnetic moment of 1.69 μ_B and an orbital magnetic moment of -0.22 μ_B (see Supplementary Fig. S1). This compares well to 2.0 μ_B and -0.38 μ_B for epitaxial V-doped Sb_2Te_3 [30]. The single-crystal studies of V-doped Sb_2Te_3 [19, 28, 31] obtain about the same magnitude of XMCD signal as Tcalev et al. [30]. The only available XMCD study with V-doped (Sb, Bi)$_2$Te$_3$ was conducted by Ye et al. who in a direct comparison find a two times smaller XMCD than in V-doped Sb_2Te_3 [31].

In Fig. 3(b–f) the XMCD signal at the V L-edge is measured as a function of magnetic field. It shows $M(H)$ curves taken at different velocities of 0.5, 1, 2, 3.8 mT/s. At the slowest speed of 0.5 mT/s, the measured coercivity H_c is 17 mT. Surprisingly, H_c increases with increasing speed up to 50 mT at 3.8 mT/s. This behavior is in line with the magnetotransport measurment of Fig. 1 where the sweep rate (~ 10 mT/s) and the coercivity (0.3 T) were higher. Similar coercivities were also reported by XMCD of V-doped Sb_2Te_3, namely 0.3 T [19] and ~ 0.15 T [28]. Intestingly, Ye et al. compared V-doped (Bi,Sb)$_2$Te$_3$ with 0%, 20%, and 30% Bi relative to Sb. The coercivity of V-doped Sb_2Te_3 was ~ 0.035 T and decreased further with increasing Bi concentration vanishing for 30% Bi [31]. Ye et al. also investigated the Dirac point by two-photon photoemission indicating that the vanishing hysteresis corresponds to the bulk insulating state (Dirac point 35 meV above E_F) [31]. Although none of the XMCD studies specified the hysteresis ramping speed, we speculate that a time-dependent relaxation could play a role here as well. In order to explore small ramping rates, i.e, long time scales, we have in Fig. 3(f) reversed the magnetic field once

to small values monitoring again the XMCD signal in reflectivity. For the largest field of $H = 20$ mT, we obtain a time scale of about 40 s in agreement with Fig. 3(e). From these data, it can be concluded that in the present experiment the magnetization decays with time. Figure 3(f) shows that this occurs on a time scale of minutes.

These observations can be related to the magnetism of Cr-doped $(Bi,Sb)_2Te_3$ which is complex and characterized by superparamagnetism [32]. A strong influence of the gate voltage on the magnetic relaxation was observed and interpreted as due to the role of charge carriers for the magnetic interaction [32]. In that case, the instability of the magnetization could be connected to the insulating state. Although the ferromagnetism of V-doped $(Bi,Sb)_2Te_3$ is much more robust than for Cr-doping (with $10\times$ higher coercivity), the electronic and magnetic effects have been found to be connected even in this material [9]. A detailed understanding of this interplay is still lacking.

The observed decay of the magnetization can directly affect the ARPES data which are measured on a much longer timescale of several minutes. Furthermore, the ARPES spectra are taken after cooling the sample down in zero field, likely resulting in superparamagnetic domains that easily relax into a random distribution. It may be that the magnetization decay prohibits the observation of the magnetic gap at the Dirac point. On the other hand, a magnetic gap of up to 90 meV can be measured by temperature-dependent ARPES in Mn-doped Bi_2Te_3 below T_C [33] as has recently been confirmed [34–36]. There are, however, important differences between the systems. The first one is the insulating character which does not apply to the strongly n-doped Mn-doped Bi_2Te_3. Another one is that the Mn-doped system avoids disorder by forming a more uniform septuple/quintuple layer $MnBi_2Te_4/Bi_2Te_3$ heterostructure [33]. In addition to the decreased disorder, this structure also enhances the exchange interaction so that the measured gap in the $MnBi_2Te_4/Bi_2Te_3$ heterostructure is about five times larger than predicted for a comparable dilute system consisting only of quintuple layers with the same Mn concentration but substituting Bi sites [37]. V-doped $(Bi,Sb)_2Te_3$ is such a dilute substitutional system and the gap may just be too small to observe in ARPES. The finding of the bulk valence band at the Fermi energy [24] may explain the limitation of the QAHE to low temperature. It cannot explain the absence of the gap at the Dirac point since it is clearly separated in ARPES data by the electron momentum parallel to the surface. Finally, the magnetism of Mn is much more localized than the one of V and this difference may also be relevant in the dilute system. This is similar to the case

of differences in the exchange splitting in elemental Fe and Ni as measured by ARPES: in the former, the exchange splitting persists above T_C whereas it vanishes in the latter. We note that in those elemental ferromagnets, the exchange splitting is maintained below T_C in magnetic domains even when a sample is cooled in zero field, resulting in the macroscopic magnetization being zero.

From recent work on Cr-doped $(Bi,Sb)_2Te_3$ [32] we learn, however, that the domain structure is not at all of the type well known from elemental Fe and Ni and this may the reason why the decay of magnetization below T_C leads to the absence of a measurable magnetic gap at the Dirac point.

In summary, we have investigated V-doped $(Bi,Sb)_2Te_3$ which is close to the QAHE by synchrotron radiation methods ARPES and XMCD using pieces from the same sample. We find that a small downward band bending occurs but no magnetic gap can be observed at the Dirac point down to T = 1 K, much below the Curie temperature of $\sim$ 25 K. The XMCD experiments which give access to the element specific magnetization of the V reveal a surprising decay of the magnetization in zerofield. This could prevent the observation of the magnetic gap at the Dirac point by ARPES. It would be very helpful to gain insight into the magnetic domain structure at temperatures of 1 K and below.

Fig. 1. (a) Longitudinal and (b,c) transversal resistance vs. magnetic field. A T_C of 25 K is derived.

Fig. 2. ARPES spectra at (a,b) 5 K and (c) the temperature dependence in normal emission ($k_\parallel = 0$ Å^{-1}) covering the range above and below the ferromagnetic phase transition. No apparent gap occurs down to 1 K. (d) The position of the Dirac point is determined from the width of the momentum distribution curves (MDC) in (b) as -50 meV. This position is marked by arrows in panels (d) and (a).

Fig. 3. (a) X-ray absorption and x-ray magnetic circular dichroism (XMCD) in total electron yield at 4 K. (b–d,f) Time dependence of XMCD hysteresis loops taken in reflectivity at 4 K. The difference of reflectivity for σ_+ and σ_- light is plotted versus the applied magnetic field H. (b–d) The ramping rate (RR) is given in the figure. (e) Plot of coercivity H_c vs. RR. (f) Alternative measurement to explore panel (e) towards longer time scales. Like in

panels (b–d) the XMCD in reflectivity is plotted. The sample was at first magnetized in the opposite direction, then the field was driven through zero to the field H indicated in the panel.

Data availability

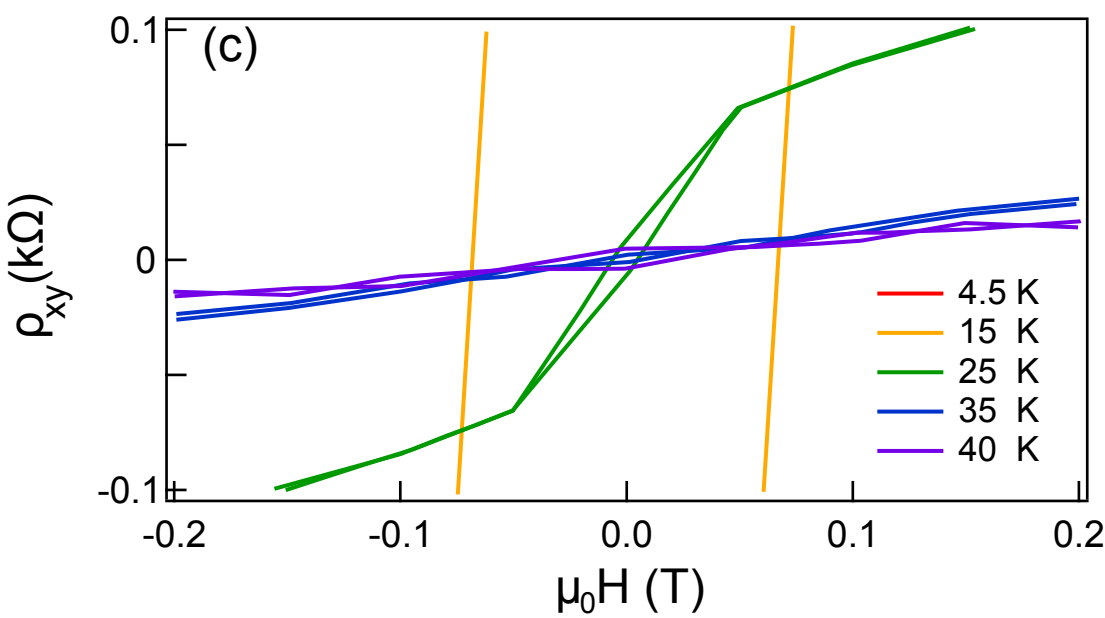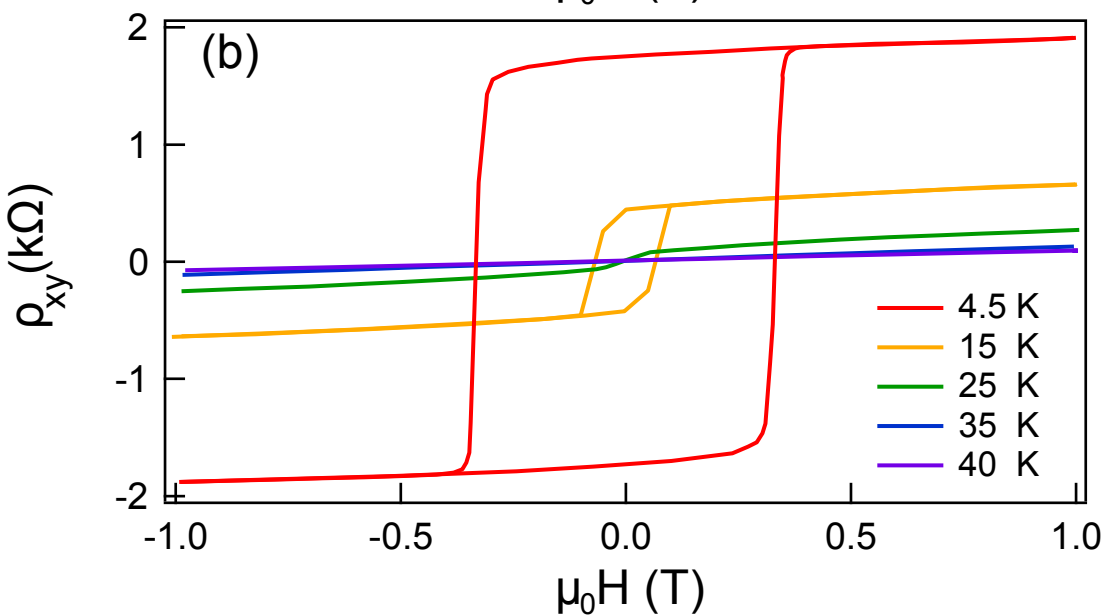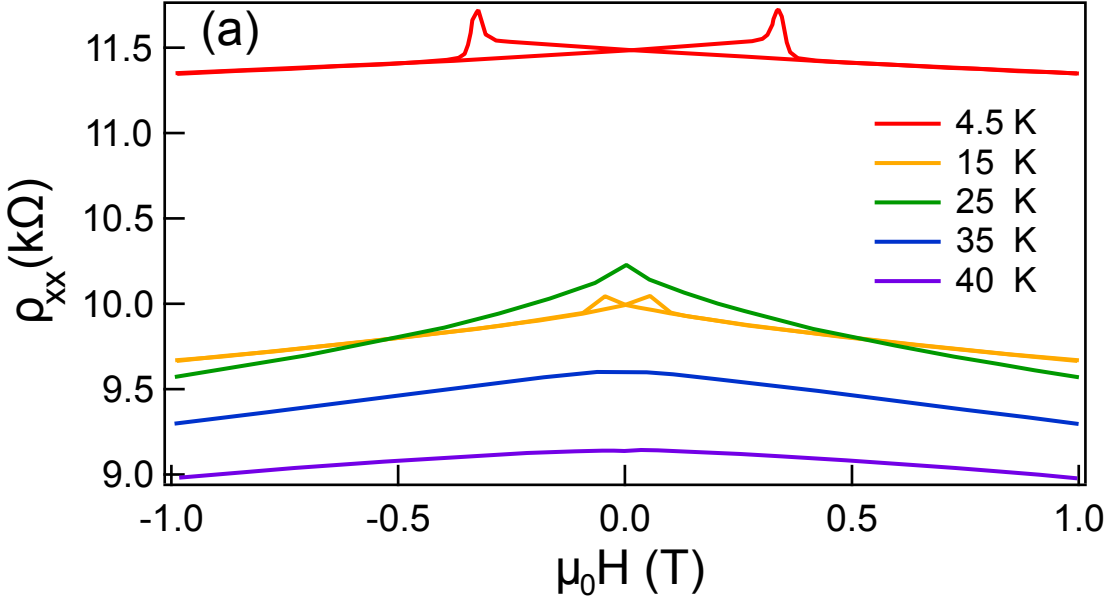The data that support the findings of this study are available from the corresponding author upon reasonable request.

[1] C.-Z. Chang et al., Experimental observation of the quantum anomalous Hall effect in a magnetic topological insulator, Science 340, 167 (2013).

[2] M. Onoda, N. Nagaosa, Quantized Anomalous Hall Effect in Two-Dimensional Ferromagnets: Quantum Hall Effect in Metals, Phys. Rev. Lett. 90, 206601 (2003).

[3] R. Yu et al., Quantized anomalous Hall effect in magnetic topological insulators, Science 329, 61 (2010).

[4] J. G. Checkelsky, R. Yoshimi, A. Tsukazaki, K. S. Takahashi, Y. Kozuka, J. Falson, M. Kawasaki, Y. Tokura, Trajectory of the anomalous Hall effect toward the quantized state in a ferromagnetic topological insulator, Nature Phys. 10, 731 (2014).

[5] X. Kou, S.-T. Guo, Y. Fan, L. Pan, M. Lang, Y. Jiang, Q. Shao, T. Nie, K. Murata, J. Tang, Y. Wang, L. He, T.-K. Lee, W.-L. Lee, K. L. Wang, Scale-Invariant Quantum Anomalous Hall Effect in Magnetic Topological Insulators beyond the Two-Dimensional Limit, Phys. Rev. Lett. 113, 137201 (2014).

[6] A. J. Bestwick, E. J. Fox, X. Kou, L. Pan, K. L. Wang, D. Goldhaber-Gordon, Precise Quantization of the Anomalous Hall Effect near Zero Magnetic Field, Phys. Rev. Lett. 114, 187201 (2015).

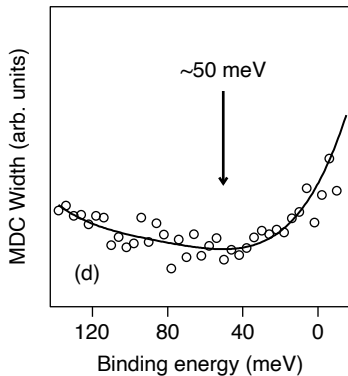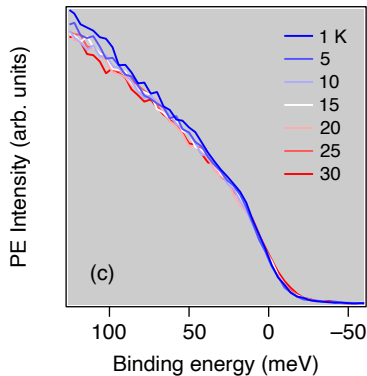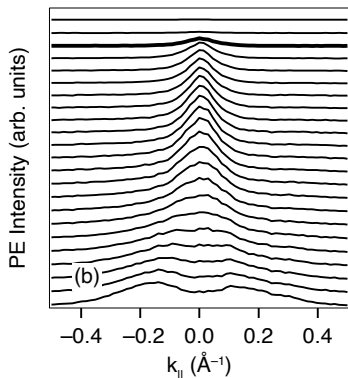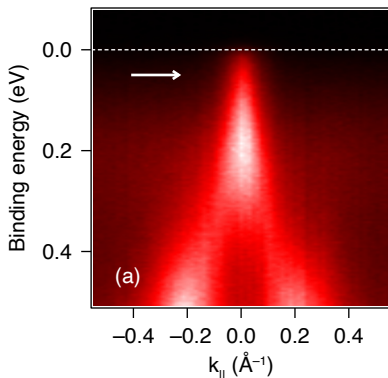[7] A. Kandala, A. Richardella, S. Kempinger, C.-X. Liu, N. Samarth, Giant anisotropic magne-

toresistance in a quantum anomalous Hall insulator, Nature Commun. 6, 7434 (2015).

[8] C.-Z. Chang, W. Zhao, D. Y. Kim, H. Zhang, B. A. Assaf, D. Heiman, S.-C. Zhang, C. Liu, M. H. W. Chan, J. S. Moodera, High-precision realization of robust quantum anomalous Hall state in a hard ferromagnetic topological insulator, Nat. Mater. 14, 473 (2015).

[9] S. Grauer, S. Schreyeck, M. Winnerlein, K. Brunner, C. Gould, L. W. Molenkamp, Coincidence of superparamagnetism and perfect quantization in the quantum anomalous Hall state, Phys. Rev. B 92, 201304(R) (2015).

[10] Z. Zhoua, C. Uher, M. Zabcik, P. Lostak, Carrier-mediated ferromagnetism in vanadium-doped $(Sb_{1-x}Bi_x)_2Te_3$ solid solutions, Appl. Phys. Lett. 88, 192502 (2006).

[11] Yi-Jiunn Chien, Ph. D. thesis, University of Michigan (2007).

[12] M. G. Vergniory, D. Thonig, M. Hoffmann, I. V. Maznichenko, M. Geilhufe, M. M. Otrokov, X. Zubizarreta, S. Ostanin, A. Marmodoro, J. Henk, W. Hergert, I. Mertig, E. V. Chulkov, A. Ernst, Exchange interaction and its tuning in magnetic binary chalcogenides, Phys. Rev. B 89, 165202 (2014).

[13] J. A. Krieger, Cui-Zu Chang, M.-A. Husanu, D. Sostina, A. Ernst, M. M. Otrokov, T. Prokscha, T. Schmitt, A. Suter, M. G. Vergniory, E. V. Chulkov, J. S. Moodera, V. N. Strocov, Z. Salman, Spectroscopic perspective on the interplay between electronic and magnetic properties of magnetically doped topological insulators, Phys. Rev. B 96, 184402 (2017).

[14] T. R. F. Peixoto, H. Bentmann, S. Schreyeck, M. Winnerlein, C. Seibel, H. Maaß, M. Al-Baidhani, K. Treiber, S. Schatz, S. Grauer, Ch. Gould, K. Brunner, A. Ernst, L. W. Molenkamp, F. Reinert, Impurity states in the magnetic topological insulator V:$(Bi,Sb)_2Te_3$, Phys. Rev. B 94, 195140 (2016).

[15] M. Götz, K. M. Fijalkowski, E. Pesel, M. Hartl, S. Schreyeck, M. Winnerlein, S., H. Scherer, K. Brunner, C. Gould, F. J. Ahlers, L. W. Molenkamp, Precision measurement of the quantized anomalous Hall resistance at zero magnetic field, Appl. Phys. Lett. 112, 072102 (2018).

[16] E. J. Fox, I. T. Rosen, Yanfei Yang, G. R. Jones, R. E. Elmquist, Xufeng Kou, Lei Pan, Kang L. Wang, and D. Goldhaber-Gordon, Part-per-million quantization and current-induced breakdown of the quantum anomalous Hall effect, Phys. Rev. B 98, 075145 (2018).

[17] C.-Z. Chang, W. Zhao, D. Y. Kim, P. Wei, J. K. Jain, C. Liu, M. H.W. Chan, J. S. Moodera, Zero-Field Dissipationless Chiral Edge Transport and the Nature of Dissipation in the Quantum Anomalous Hall State, Phys. Rev. Lett. 115, 057206 (2015).
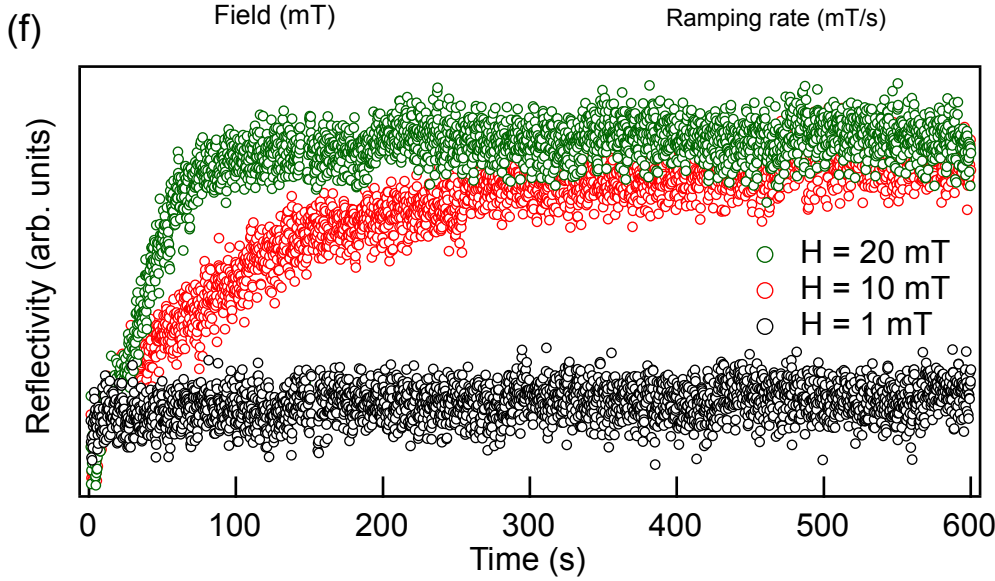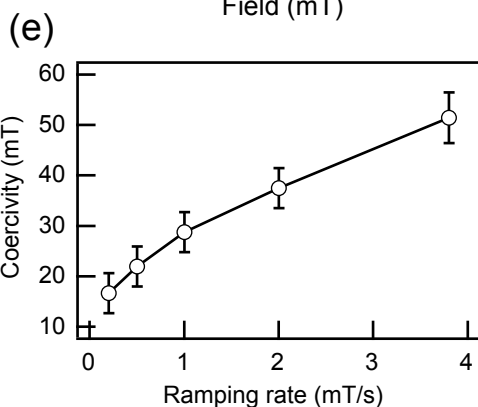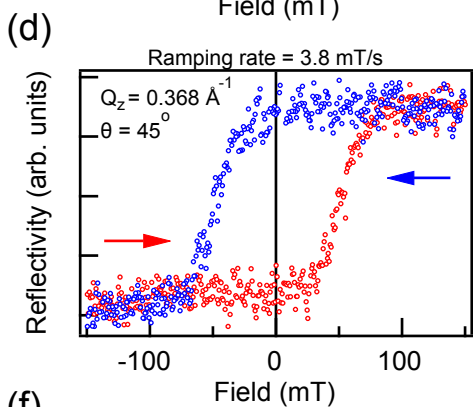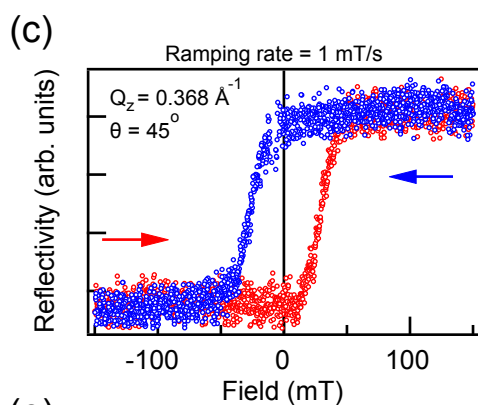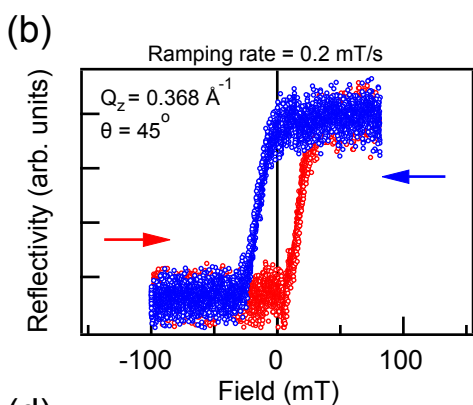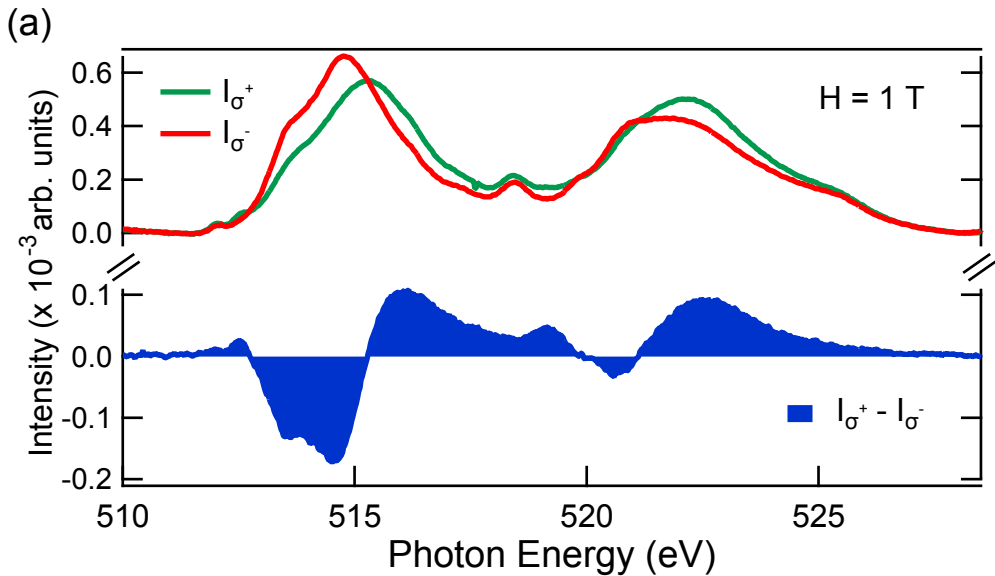
[18] M. Mogi, R. Yoshimi, A. Tsukazaki, K. Yasuda, Y. Kozuka, K. S. Takahashi, M. Kawasaki, Y. Tokura, Magnetic modulation doping in topological insulators toward higher-temperature quantum anomalous Hall effect, Appl. Phys. Lett. 107, 182401 (2015).

[19] P. Sessi, R. R. Biswas, T. Bathon, O. Storz, S. Wilfert, A. Barla, K. A. Kokh, O. E. Tereshchenko, K. Fauth, M. Bode, A. V. Balatsky, Dual nature of magnetic dopants and competing trends in topological insulators, Nat. Commun. 7, 12027 (2016).

[20] I. Lee, C. K. Kim, J. Lee, S. J. L. Billinge, R. Zhong, J. A. Schneeloch, T. Liu, T. Valla, J. M. Tranquada, G. Gu, J. C. S. Davis, Imaging Dirac-mass disorder from magnetic dopant atoms in the ferromagnetic topological insulator $Cr_x(Bi_{0.1}Sb_{0.9})_{2-x}Te_3$, Proc. Natl. Acad. Sci. U. S. A. 112, 1316 (2015).

[21] Cui-Zu Chang, Peizhe Tang, Yi-Lin Wang, Xiao Feng, Kang Li, Zuocheng Zhang, Yayu Wang, Li-Li Wang, Xi Chen, Chaoxing Liu, Wenhui Duan, Ke He, Xu-Cun Ma, and Qi-Kun Xue, Chemical-Potential-Dependent Gap Opening at the Dirac Surface States of Bi_2Se_3 Induced by Aggregated Substitutional Cr Atoms, Phys. Rev. Lett. 112, 056801 (2014).

[22] L. Zhang, D. Zhao, Y. Zang, Y. Yuan, G. Jiang, M. Liao, D. Zhang, K. He, X. Ma, Q. Xue, Ferromagnetism in vanadium-doped Bi_2Se_3 topological insulator films, APL Mater. 5, 076106 (2017).

[23] C. Riha, B. Düzel, K. Graser, O. Chiatti, E. Golias, J. Sánchez-Barriga, O. Rader, O. E. Tereshchenko, S. F. Fischer, Electrical Transport Properties of Vanadium-Doped $Bi_2Te_{2.4}Se_{0.6}$, phys. stat. sol. (b) 256, 2000088 (2021).

[24] W. Li, M. Claassen, C.-Z. Chang, B. Moritz, T. Jia, C. Zhang, S. Rebec, J. J. Lee, M. Hashimoto, D.-H. Lu, R. G. Moore, J. S. Moodera, T. P. Devereaux, Z.-X. Shen, Origin of the low critical observing temperature of the quantum anomalous Hall effect in V-doped (Bi, Sb)$_2$Te$_3$ film, Sci. Rep. 6, 32732 (2016

[25] C. K. Kim, J. D. Denlinger, A. K. Kundu, G. Gu, T. Valla, Absence of a Dirac gap in ferromagnetic $Cr_x(Bi_{0.1}Sb_{0.9})_{2-x}Te_3$, J. Appl. Phys. 129, 083902 (2021).

[26] X.-L. Qi, T. L. Hughes, S.-C. Zhang, Topological field theory of time-reversal invariant insulators, Phys. Rev. B 78, 195424 (2008).

[27] G. Rosenberg, M. Franz, Surface magnetic ordering in topological insulators with bulk magnetic dopants, Phys. Rev. B 85, 195119 (2012).

[28] M. F. Islam, C. M. Canali, A. Pertsova, A. Balatsky, S. K. Mahatha, C. Carbone, A. Barla,

K. A. Kokh, O. E. Tereshchenko, E. Jiménez, N. B. Brookes, P. Gargiani, M. Valvidares, S. Schatz, T. R. F. Peixoto, H. Bentmann, F. Reinert, J. Jung, T. Bathon, K. Fauth, M. Bode, and P. Sessi, Systematics of electronic and magnetic properties in the transition metal doped Sb_2Te_3 quantum anomalous Hall platform, Phys. Rev. B 97, 155429 (2018).

[29] C. T. Chen, Y. U. Idzerda, H.-J. Lin, N. V. Smith, G. Meigs, E. Chaban, G. H. Ho, E. Pellegrin, and F. Sette, Experimental Confirmation of the X-Ray Magnetic Circular Dichroism Sum Rules for Iron and Cobalt, Phys. Rev. Lett. 75, 152 (1995).

[30] A. Tcakaev, V. B. Zabolotnyy, R. J. Green, T. R. F. Peixoto, F. Stier, M. Dettbarn, S. Schreyeck, M. Winnerlein, R. Crespo Vidal, S. Schatz, H. B. Vasili, M. Valvidares, K. Brunner, C. Gould, H. Bentmann, F. Reinert, L. W. Molenkamp, and V. Hinkov, Comparing magnetic ground-state properties of the V- and Cr-doped topological insulator $(Bi,Sb)_2Te_3$, Phys. Rev. B 101, 045127 (2020).

[31] M. Ye, T. Xu, G. Li, S. Qiao, Y. Takeda, Y. Saitoh, S.-Y. Zhu, M. Nurmamat, K. Sumida, Y. Ishida, S. Shin, and A. Kimura, Negative Te spin polarization responsible for ferromagnetic order in the doped topological insulator $V_{0.04}(Sb_{1-x}Bi_x)_{1.96}Te_3$, Phys. Rev. B 99, 144413 (2019).

[32] E. O. Lachman, A. F. Young, A. Richardella, J. Cuppens, H. R. Naren, Y. Anahory, A. Y. Meltzer, A. Kandala, S. Kempinger, Y. Myasoedov, M. E. Huber, N. Samarth, E. Zeldov, Visualization of superparamagnetic dynamics in magnetic topological insulators, Sci. Adv. 1, e1500740 (2015).

[33] E. D. L. Rienks, S. Wimmer, J. Sánchez-Barriga, O. Caha, P. S. Mandal, J. Růžička, A. Ney, H. Steiner, V. V. Volobuev, H. Groiss, M. Albu, G. Kothleitner, J. Michalicka, S. A. Khan, J. Minár, H. Ebert, G. Bauer, F. Freyse, A. Varykhalov, O. Rader, G. Springholz, Large magnetic gap at the Dirac point in $Bi_2Te_3/MnBi_2Te_4$ heterostructures, Nature 576, 423 (2019)

[34] I. I. Klimovskikh, M. M. Otrokov, D. Estyunin, S. V. Eremeev, S. O. Filnov, A. Koroleva, E. Shevchenko, V. Voroshnin, A. G. Rybkin, I. P. Rusinov et al., Tunable 3D/2D magnetism in the $(MnBi_2Te_4)(Bi_2Te_3)_m$ topological insulators family, npj Quantum Materials 5, 54 (2020).

[35] R. Lu, H. Sun, S. Kumar, Y. Wang, M. Gu, M. Zeng, Y.-J. Hao, J. Li, J. Shao, X.-M. Ma et al., Half-Magnetic Topological Insulator with Magnetization-Induced Dirac Gap at a Selected Surface, Phys. Rev. X 11, 011039 (2021).

[36] C. X. Trang, Q. Li, Y. Yin, J. Hwang, G. Akhgar, I. Di Bernardo, A. Grubišić-Čabo, A. Tadich, M. S. Fuhrer, S.-K. Mo, N. V. Medhekar, M. T. Edmonds, Crossover from 2D Ferromagnetic Insulator to Wide Band Gap Quantum Anomalous Hall Insulator in Ultrathin $MnBi_2Te_4$, ACS Nano 15, 13444 (2021).

[37] J. Henk, M. Flieger, I. V. Maznichenko, I. Mertig, A. Ernst, S. V. Eremeev, E. V. Chulkov, Topological Character and Magnetism of the Dirac State in Mn-Doped Bi_2Te_3, Phys. Rev. Lett. 109, 076801 (2012).

(a) Binding energy (eV) vs $k_{\parallel}$ (Å^{-1})

(b) PE Intensity (arb. units) vs $k_{\parallel}$ (Å^{-1})

(c) PE Intensity (arb. units) vs Binding energy (meV)
1 K
5
10
15
20
25
30

(d) MDC Width (arb. units) vs Binding energy (meV)
~50 meV

(a) Plot showing Intensity (× 10⁻³ arb. units) versus Photon Energy (eV), with I_{σ^+} (green), I_{σ^-} (red), and $I_{\sigma^+} - I_{\sigma^-}$ (blue), at H = 1 T.

(b) Ramping rate = 0.2 mT/s, $Q_z = 0.368$ Å⁻¹, $\theta = 45°$.

(c) Ramping rate = 1 mT/s, $Q_z = 0.368$ Å⁻¹, $\theta = 45°$.

(d) Ramping rate = 3.8 mT/s, $Q_z = 0.368$ Å⁻¹, $\theta = 45°$.

(e) Coercivity (mT) versus Ramping rate (mT/s).

(f) Reflectivity versus Time (s) for H = 20 mT (green), H = 10 mT (red), H = 1 mT (black).

Magnetization relaxation and search for the magnetic gap in bulk-insulating V-doped (Bi, Sb)$_2$Te$_3$

E. Golias, E. Weschke, T. Flanagan, E. Schierle, A. Richardella, E. D. L. Rienks, P. S. Mandal, A. Varykhalov, J. Sánchez-Barriga, F. Radu, N. Samarth, O. Rader
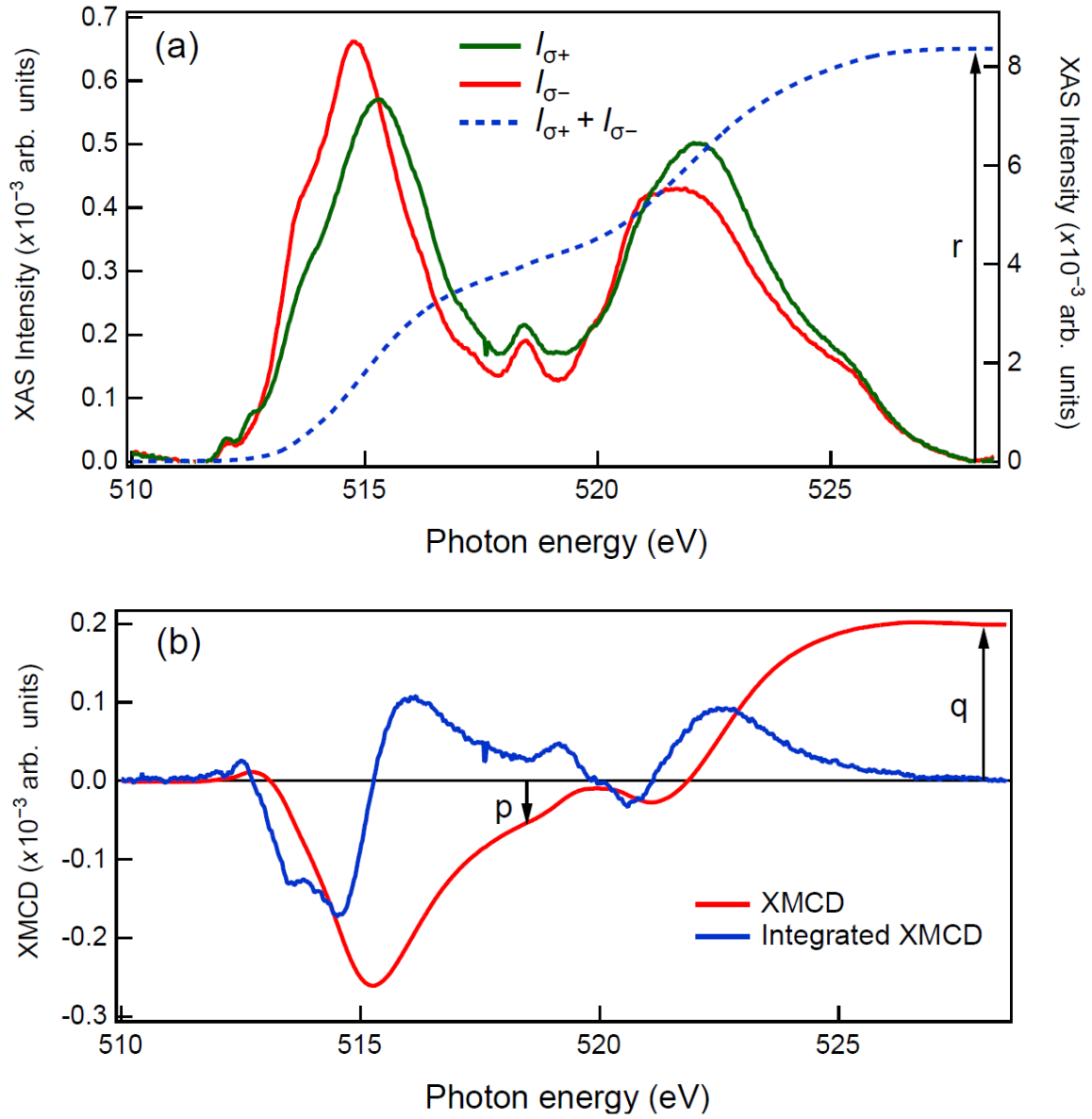

Fig. S1. XMCD spectra from Fig. 1 for sum-rule analysis. (a) X-ray absorption spectra (XAS) for the two circular polarization conditions and (b) their difference, i. e., the XMCD. Values p, q, and r as defined in C. T. Chen et al. [29] are marked.